Revision_2

Static positional disorder in ulvöspinel: A single-crystal neutron diffraction study

G. Diego Gatta[1], Ferdinando Bosi[2], Garry J. McIntyre [3], Ulf Hålenius[4]

[1] Dipartimento di Scienze della Terra, Università degli Studi di Milano, Via Botticelli 23, I-20133 Milano, Italy

[2] Dipartimento di Scienze della Terra, Sapienza Università di Roma, P.le A. Moro 5, I-00185 Roma, Italy

[3]Australian Nuclear Science and Technology Organisation, Locked Bag 2001, Kirrawee DC NSW 2232, Australia

[4] Department of Geosciences, Swedish Museum of Natural History, Box 50007, 10405 Stockholm, Sweden

Abstract

A single-crystal neutron diffraction study of a synthetic ulvöspinel sample of composition $Fe^{3+}_{0.40}Fe^{2+}_{1.80}Ti_{0.80}O_4$ was performed to investigate the static positional disorder at the octahedrally coordinated *M* site. Anisotropic structural refinement was performed in the space group $Fd\bar{3}m$ against neutron Laue diffraction data collected at 298 K from two millimetric-sized crystals. Initial structure refinements were conducted with Fe and Ti sharing the *M* site (at 1/2, 1/2, 1/2), and their partial site occupancy was refined. The tetrahedrally coordinated *T* site (at 1/8, 1/8, 1/8) was modeled as fully occupied by Fe. For both crystals, the final R_1 index was about 3% for 9 refined parameters and 129 unique reflections, with no significant residuals.

As the atomic displacement factors obtained were anomalously high, according to the previous experimental findings, F_{obs}- and ($F_{obs} - F_{cal}$)-difference Fourier maps of the nuclear density were generated. Fourier maps showed a significant minimum located out-of-center of the *M* site, and indicating a displacement of the Ti^{4+} from the center of the octahedron. A further test refinement was successfully conducted with two mutually exclusive sites: ^{M}Ti out-of-center (at 0.49, 0.49, 0.49) and ^{M}Fe on the center (at 1/2, 1/2,

1/2). The resulting displacement of Ti from the octahedral center appears to be shorter than 0.15 Å.

Using bond-valence theory, the out-of-center distortion of $^{M}Ti^{4+}$ is interpreted as a result of intrinsic distortions in the ulvöspinel structure. The potential implication of the octahedral distortion on the behavior of ulvöspinel at non-ambient conditions is discussed.

Keywords: ulvöspinel, crystal chemistry, neutron Laue diffraction, static positional disorder, bond valence theory.

Introduction

Multiple oxides with spinel structure occur as common accessory in many crustal rocks, but are expected to be important components of the Mantle assemblages. Their crystal structure and crystal chemistry, along with their thermo-elastic and magnetic behavior in response to the applied pressure (*P*) and temperature (*T*), have been the subject of a significant number of experiments for petrological and geophysical implications along with potential technological applications. The general formula of spinels is AB_2O_4, where "*A*" and "*B*" represent respectively either bivalent and trivalent cations (giving $A^{2+}B^{3+}{}_2O_4$) or tetravalent and bivalent cations (giving $A^{4+}B^{2+}{}_2O_4$). The crystal structure of spinels can be described as a slightly distorted cubic close-packed array of anions, in which the *A* and *B* cations are distributed over one eighth of all tetrahedrally coordinated (*T*) and half of all octahedrally coordinated (*M*) sites. This cation distribution leads to two types of site populations: 1) the "normal" one, where the *A* cation occupies the *T* site and the two *B* cations occupy the *M* sites; 2) the "inverse" one, where the *A* cation is ordered at *M* and the *B* cations occupy both *T* and *M* (Barth and Posnjak 1932). The spinel structure is cubic (space group $Fd\bar{3}m$). The tetrahedrally coordinated cations are located at the special positions 8*a* (Wyckoff notation; point symmetry $\bar{4}3m$) and the octahedrally coordinated cations are located at the special position 16*d* (point symmetry $\bar{3}m$), the oxygen atoms lie at the special position 32*e* (point symmetry 3*m*). The oxygen fractional coordinate (*u*) is the only variable atomic position in the structure.

Ulvöspinel is an inverse spinel, with structural formula $^{T}(Fe^{2+})^{M}(Fe^{2+}Ti^{4+})O_4$. Often, natural Ti-rich spinels belong to the solid solution between magnetite, $^{T}(Fe^{3+})^{M}(Fe^{2+}Fe^{3+})O_4$, and ulvöspinel (Akimoto 1954). A significant number of experiments have been devoted to the site allocation of cations along the magnetite-

ulvöspinel join (*e.g.*, Akimoto 1954; Chevallier et al. 1955; Néel 1955; O'Reilly and Banerjee 1965; Fujino 1974; Stout and Bayliss 1980; Sedler et al. 1994; Wechsler et al. 1984; Gatta et al. 2007; Bosi et al. 2008, 2009; Lenaz and Princivalle 2011). The most recent experimental findings suggest that Ti^{4+} is fully ordered at the *M* site, whereas Fe^{2+} and Fe^{3+} show a site preference for *M* and *T*, respectively, resulting in a slight Fe^{2+}-Fe^{3+} disorder over the *T* and *M* sites.

A series of *in situ* high-pressure experiments have recently been performed on ulvöspinel terms by single-crystal and powder X-ray diffraction and Raman spectroscopy (*e.g.*, Yamanaka et al. 2009, 2013; Kyono et al. 2011). In response to the applied pressure, ulvöspinel undergoes several phase transitions, and the transition pressure is governed by the Ti^{4+} content. For the composition Fe_2TiO_4, the stability field of the cubic polymorph ($Fd\bar{3}m$) was observed to be 0.0001-9 GPa. At P ~9 GPa, a cubic-to-tetragonal phase transition occurs; the stability of the tetragonal polymorph ($I4_1/amd$) was observed to be 9-12 GPa. At P ~12 GPa, a further phase transformation occurs from tetragonal to orthorhombic symmetry (*Cmcm*). The orthorhombic polymorph appears to be stable at least up 50 GPa, where evidence of a further transition (likely toward a *Pmma* post-spinel phase) was observed (Yamanaka et al. 2013). X-ray emission spectra of Fe*K*β collected at high pressure provided evidence of change of the spin state of Fe from high to low with increasing pressure, and at $P > 30$ GPa the fraction of high-spin Fe appeared to be negligible (Yamanaka et al. 2013). The tetragonal polymorph is only observed for Ti^{4+} contents higher than 0.62 atoms per formula unit (apfu, normalized to 4 oxygen atoms). For lower contents, the tetragonal form does not occur and a cubic-to-orthorhombic phase transition occurs in response to the applied pressure. A *P versus* composition phase diagram of ulvöspinel is reported by Yamanaka et al. (2009). A recent *in situ* high-pressure Raman study confirmed the experimental findings previously reported (Kyono et al. 2011). A cubic-to-tetragonal phase transition was also observed at low temperature by *in situ* single-crystal X-ray diffraction: Yamanaka et al. (2009) observed a transition from $Fd\bar{3}m$ to $I4_1/amd$ symmetry at $T < 160$ K. Surprisingly, the mechanisms that govern the transition to the low-*T* and to the high-*P* tetragonal polymorphs appear to be different: in the low-*T* polymorph, the unit-cell parameter ratio $c/a > 1$, whereas in the high-*P* polymorph $c/a < 1$. The authors explain such a difference with a different degeneracy of the *e* orbit of the Fe^{2+} at the *T* site (*i.e.*, Jahn-Teller effect).

Previous experiments on ulvöspinel terms, based on high-quality structure refinements (*e.g.*, Wechsler et al. 1984; Bosi et al. 2009), suggested the likely presence of a

static positional disorder due to the mixing of Fe^{2+} and Ti^{4+} over the *M*-sites. This would explain the atypical relatively large displacement parameters, when compared to those obtained for other spinels at comparable *T/P* conditions. Local violation of the cubic symmetry was also considered, on the basis of diffuse scattering observed in neutron powder diffraction patterns (Wechsler et al. 1984). However, the out-of-center distortion around the octahedrally coordinated Ti^{4+} cation (e.g., Kunz and Brown 1995) in the highly-symmetric spinel structure has never been taken into account in the literature.

The aim of this study is a re-investigation of the crystal structure of a synthetic ulvöspinel (sample FeTib3 in Bosi et al. 2009) by single-crystal neutron Laue diffraction in order to explore the notion of an out-of-center distortion of the octahedron. The structure of sample FeTib3 was already characterized using single-crystal X-ray diffraction, and chemical analysis resulted in the structural formula $^{T}(Fe^{2+}_{0.87}Fe^{3+}_{0.13})_{\Sigma 1.00}{}^{M}(Fe^{2+}_{0.93}Fe^{3+}_{0.27}Ti_{0.80})_{\Sigma 2.00}O_4$ (Bosi et al. 2009). Unlike X-rays, the neutron structure refinement is expected to provide a better description of atomic displacement around the equilibrium position, as neutrons are scattered by the nuclei rather than the electrons, and so the scattering power does not fall off with angle, making possible measurements at high values of $\sin\theta/\lambda$. In addition, the neutron scattering lengths of Fe (9.45 fm) and Ti (-3.438 fm) (Sears 1986) are significantly different, making single-crystal neutron diffraction the best experimental technique to answer the open questions about the crystal structure/chemistry of ulvöspinel.

Experimental methods

Synthesis and chemical analysis

The spinel single crystals used in the present work were synthesized by flux-growth methods at controlled oxygen fugacities and at temperatures between 1200-900 °C (Bosi et al. 2008, 2009). The chemical composition of the crystals was characterized by electron microprobe in wavelength-dispersive mode (EMPA-WDS) and Mössbauer spectroscopy (Bosi et al. 2009).

Single-crystal X-ray and neutron diffraction experiments

Two relatively large crystals of sample FeTib3 with octahedral form were selected for the neutron diffraction experiments. The unit-cell parameter (*a*) of the ulvöspinel sample FeTib3 was previously determined by X-ray diffraction on a single-crystal of about $0.13 \times 0.13 \times 0.13$ mm^3 at room temperature, with a Siemens P4 four-circle diffractometer

(Mo*K*α radiation, point detector), on the basis of 52 reflections in the range 85–95 °2θ (Bosi et al. 2009): a = 8.5139(5) Å (Table 1).

Neutron Laue data were collected at 298 K from the two crystals on the Laue diffractometer VIVALDI at the Institute Laue-Langevin in Grenoble (France). VIVALDI uses the Laue diffraction technique on an unmonochromated thermal-neutron beam with a large solid-angle (8 sterad) cylindrical image-plate detector, in order to increase the detected diffracted intensity by one-to-two orders of magnitude compared with a conventional monochromatic experiment (McIntyre et al. 2006). Each crystal was mounted with the high-symmetry axes well away from the single instrument rotation axis, in order to avoid bias in the final refined anisotropic displacement parameters due to the blind region in reciprocal space around the rotation axis. A total of 30 Laue diffraction patterns for crystal #1 and 19 for crystal #2, each accumulated over 15 min on average, were collected at 15° intervals in rotation of the crystal perpendicular to the incident neutron beam. The diffraction data from both crystals extended to a minimum d spacing of ~0.5 Å.

The Laue patterns were indexed using the program LAUEGEN (Daresbury Laboratory Laue Suite, Campbell 1995, Campbell et al. 1998), and the reflections integrated using the program INTEGRATE+ which uses a two-dimensional version of the minimum σ(I)/I algorithm (Wilkinson et al. 1988). Correction for absorption was deemed unnecessary in view of the low absorption coefficients of the constituent elements. The reflections were normalized for the incident wavelength, using a curve derived by comparing equivalent reflections and multiple observations, and corrected for the different angles of incidence via the program LAUE4 (Piltz 2012). Reflections were observed with wavelengths between 0.78 Å and 5.20 Å, but just those with wavelengths in the range 0.85 Å to 1.70 Å were taken through normalization to a common wavelength. A total of 8338 and 5550 reflections were collected for crystals #1 and #2, respectively, and yielded 135 and 134 unique reflections in space group $Fd\bar{3}m$ (Table 1). No significant evidence of diffuse scattering was observed, as previously reported by Wechsler et al. (1984).

A further data collection was performed at lower temperatures, with the aim to describe the structure evolution of the ulvöspinel down to 10 K. However, at T < 140 K the diffraction spots broadened, indicative of an impending phase transition. This was expected on the basis of the previous results by Yamanaka et al. (2009). However, the Bragg reflections did not clearly split into multiple spots, which makes identifying whether the symmetry is lowered difficult. This hindered a low-T study of ulvöspinel.

Structure refinement

The intensity data of the two ulvöspinel crystals were processed with the suite of programs implemented in the WinGX package (Farrugia 1999). The normalized structure factors, their statistics of distributions along with the reflection conditions were fully consistent with the space group $Fd\bar{3}m$. The anisotropic crystal-structure refinements were then conducted using the SHELX-97 software (Sheldrick 2008), starting from the X-ray structural model of Bosi et al. (2009). The neutron scattering lengths of Fe, Ti, and O used were those according to Sears (1986). The secondary isotropic extinction was modeled according to Larson (1967), as implemented in the SHELXL-97 package. The structure refinements were conducted with Fe and Ti sharing the *M* site at (1/2, 1/2, 1/2), and their partial site occupancy was refined. The *T* site at (1/8, 1/8, 1/8) was modeled as fully occupied by Fe. With this structure model, convergence was rapidly achieved and the variance-covariance matrix showed no significant correlations between the refined parameters. At the end of the last cycle of the two refinements, no peak larger than ±0.6 fm/Å^3 was present in the final difference-Fourier map of the nuclear density (Table 1). The final disagreement index (R_1) was 0.0312 (crystal #1) and 0.0324 (crystal #2) for 9 refined parameters and 129 unique reflections with $F_{obs} > 4\sigma(F_{obs})$ (Table 1). Site coordinates, site occupancies, atomic displacement parameters and bond lengths are reported in Table 1. A CIF is deposited.

As the atomic displacement factor for the *M* site obtained in both the refinements was anomalously large, in accordance with the previous experimental findings (*e.g.*, Wechsler et al. 1984; Bosi et al. 2009), F_{obs}- and ($F_{obs} - F_{cal}$)-difference Fourier maps of the nuclear density were generated. The ($F_{obs} - F_{cal}$) function was phased on the basis of a structure model *without* the *M* site. The F_{obs} map showed a significant minimum between 0.46-0.48, 0.46-0.48, 0.46-0.48. The ($F_{obs} - F_{cal}$) map showed a minimum at approximately 0.485-0.495, 0.485-0.495, 0.485-0.495 (Fig. 1). As Ti has a negative scattering length (Sears 1986), a test refinement was conducted with Ti at the position (0.49, 0.49, 0.49) and Fe at (1/2, 1/2, 1/2), with partial site occupancy. However, the refinement led to a convergence of Ti and Fe at (1/2, 1/2, 1/2). A further test refinement was then conducted on crystal #1 fixing the coordinates of Ti at (0.49, 0.49, 0.49), and using an isotropic displacement factor (U_{iso}). With this configuration, convergence was rapidly achieved. The quality of the refinement, deduced by the R_1 index and residuals, was almost identical to

that with Fe and Ti sharing the *M* site at (1/2, 1/2, 1/2) (Table 1). However, the correlations between some of the refined parameters, in the variance-covariance matrix, were high. We then fixed, in the last cycles of refinement, the U_{iso}(Ti) value, as it was similar to that previously obtained for the *M* site (Table 1), so reducing the correlation. With this structure model, Ti was refined to ~0.87 apfu (Table 1). The difference-Fourier map of the nuclear density at z = 0.49 with a structure model with Fe at (1/2, 1/2, 1/2) and Ti at (0.49, 0.49, 0.49) is shown in Fig. 1. Fixing the Ti coordinates at (0.48, 0.48, 0.48) or (0.47, 0.47, 0.47) led to physically unacceptable displacement parameters.

Results and Discussion

To the best of our knowledge, this is the first experiment in which the crystal structure of ulvöspinel is investigated on the basis of single-crystal neutron diffraction data. The neutron structure refinements (crystals #1 and #2) with Fe and Ti sharing the *M* site lead to a refined fraction of Ti of 0.86-0.88 apfu. If Ti is dislocated to the position (0.49, 0.49, 0.49), the refined fraction of Ti is ~0.87 apfu (Table 1). The difference between the amounts of Ti derived from the electron microprobe analysis (~0.80 apfu, Bosi et al. 2009) and the neutron structure refinements is acceptable.

The structure refinements conducted with Ti and Fe sharing the *M* sites confirm the experimental findings previously reported for ulvöspinel (*e.g.*, Wechsler et al. 1984; Bosi et al. 2009), with atomic displacement parameters generally higher than those observed for spinels at the same temperature. The nuclear density maps provide the only evidence of a static positional disorder over the *M* sites of the spinel structure, due to size and charge mismatch between Ti^{4+} and Fe^{2+}. Refinements with fixed Ti coordinate at (0.49, 0.49, 0.49) and isotropic displacement parameter was successful, but unconstrained refinements with Ti out-of-center of the octahedron moved it to the position (1/2, 1/2, 1/2). This is due to the short interatomic distance $^{M}Ti^{4+}$-$^{M}Fe^{2+}$ of ~0.15 Å (Fig. 2, Table 1). The relative large atomic displacement parameters indicate that a positional disorder at the *M* site in ulvöspinel may occur at room temperature along with an out-of-center location of ^{M}Ti. The latter, however, is not pronounced enough to be detected by an "unrestrained" structural refinement. As a consequence, the figures of merit of the refinements conduced with and without out-of-center Ti site are not significantly different (Table 1).

A bond valence approach to ulvöspinel

In their paper on out-of-center distortion of octahedrally coordinated d^0 transition metals, Kunz and Brown (1995) showed that electronic distortion of Ti^{4+} (also known as second-order Jahn-Teller distortion) is of moderate strength, and *only* occurs if structural distortions are present. These latter distortions can be related to the topology of the bond graph and steric strains (*e.g.*, cation-cation repulsion) (Brown 2009). The presence of structural distortions in ulvöspinel can be analyzed by using bond-valence theory.

In general, the topology of a structure can be represented by a bond network in which ions are represented by the nodes of a graph and bonds by the links between them (*e.g.*, Brown 2002, 2009). This topology is dictated by two network equations called valence-sum rule, $\sum_j S_{ij} = Vi$, and equal-valence rule, $\sum_{\text{loop}} S_{ij} = 0$ (where Vi is the atomic valence of the atom i and, S_{ij} is the bond valence between the atoms i and j). The former rule requires that at each atom the sum of the bond valences equal the atom valence, the latter rule represents the condition that each atom distributes its valence equally among its bonds subject to the constraint of valence-sum rule (*e.g.*, Kunz and Brown 1995; Brown 2002). As the valence-sum rule is a more stringent requirement than the equal-valence rule, the bond network can be distorted: *i.e.*, non-equivalent bonds may occur around an atom to maintain the bond-valence sums equal to the atom valence. Theoretical bond valences can be derived from the solution of network equations.

The bond network for the ulvöspinel topology $[^{T}(Fe^{2+})^{M}(Fe^{2+}Ti^{4+})O_4]$ can be treated as an array of atomic valences, which are equal to the formal ionic point charges (Brown 2002). This bond network can lead to two different scenarios regarding the *M* sites: 1) random distribution of Fe^{2+} and Ti^{4+}, where the atomic valences 2+ and 4+ occur in equal amounts at the *M* sites yielding a mean valence of 3+ (Fig 3a); 2) ordered distribution of Fe^{2+} and Ti^{4+}, where the valence 2+ occurs at one *M* site (the *M*1 subsite) and the valence 4+ occurs at the other *M* site (the *M*2 subsite) (Fig. 3b). In 1) the two *M*-sites show equivalent bond valences (0.50 × 6 valence units, vu), thus no distortions are expected to occur in their environment. This scenario may be referred to as long-range cubic structure of the ulvöspinel ($Fd\bar{3}m$), with static positional disorder as determined from the diffraction techniques. Conversely, in 2) *M*1 and *M*2 show non-equivalent bond valences (0.36 × 4 vu and 0.27 × 2 vu for *M*1; 0.63 × 4 vu and 0.73 × 2 vu for *M*2), thus distorted environments may occur. This scenario may represent either a long-range structure with a reduction in symmetry due to a cation order (*e.g.*, $P4_122$ tetragonal-phase of Zn_2TiO_4, Millard et al. 1995) or a short-range structure of ulvöspinel which would show statistical disorder to conform with the long range cubic symmetry. Therefore, the symmetric and undistorted

bond network of ulvöspinel at the long-range scale is in fact locally distorted. It is important to note that one can predict distorted environments only on the basis of the distribution of the atomic valences over the crystallographic sites, but the occurrence of distorted bond lengths will also depend on the electron configuration of cation: *e.g.*, the electron state of Ti^{4+} or V^{5+} favors distorted octahedral environments, whereas that of Fe^{2+} or Sn^{4+} not (*e.g.*, Kunz and Brown 1995).

Concerning the distortion caused by cation-cation repulsion at the *M*-sites, the magnitude of the cation-cation repulsion (*e.g*, the repulsion $^{M}Ti^{4+}$-$^{M}Ti^{4+}$ is stronger than that of the $^{M}Fe^{2+}$- $^{M}Fe^{2+}$) is not expected to play an important role. In contrast, its asymmetry can control the direction of the out-of-center distortion of Ti^{4+} (Kunz and Brown 1995). In the spinel structure, the octahedra share half of their edges in such a way that an *M* site is surrounded by six (3+3) *M* sites in accordance with the $\bar{3}$ symmetry. Thus, the long-range structure shows a symmetric configuration of the shared edges that cancels that cation-cation repulsion leaving Ti^{4+} in the center of its octahedron. However, the situation appears to be different at the short-range scale. In order to have a cation-cation repulsion that activates a displacement of the Ti^{4+} from the center of its octahedron, asymmetric Fe^{2+}-Ti^{4+} arrangements around Ti^{4+} would occur. In this regard, it is interesting to look at the short-range cation arrangements involved in ulvöspinel. The O site is coordinated by cations at the (*T* + 3*M*) sites. Disregarding the *T* site, which is solely occupied by Fe^{2+}, four possible local arrangements involving *M*-cations around O are expected: $^{M}(3Fe^{2+})$, $^{M}(3Ti)$, $^{M}(2Fe^{2+} + Ti)$ and $^{M}(Fe^{2+} + 2Ti)$. From these arrangements, asymmetric distributions of the charges around the Ti^{4+} can be obtained (Fig. 4): $(Fe\text{-}Fe\text{-}Fe)^{\Sigma 6+}$-$(Ti^{4+})$-$(Ti\text{-}Ti\text{-}Ti)^{\Sigma 12+}$ or $(Fe\text{-}Fe\text{-}Ti)^{\Sigma 8+}$-$(Ti^{4+})^{+}$-$(Fe\text{-}Ti\text{-}Ti)^{\Sigma 10+}$. Such asymmetry may therefore force the Ti away from the center of the octahedron so that the Ti^{4+} local environment is distorted.

In summary, the out-of-center distortion of $^{M}Ti^{4+}$ is favored at the local scale, where asymmetries in both bond network and cation-cation repulsion can occur. The absence of any source of structural distortions would result in Ti^{4+} being in a undistorted environment, but the presence of these intrinsic asymmetries (distortions) and the second-order Jahn-Teller distortion of Ti^{4+}, which are mutually supportive (Kunz and Brown 1995), allows its displacement from the position (1/2, 1/2, 1/2) to (0.49, 0.49, 0.49) in the ulvöspinel sample FeTib3 (Fig. 2). In addition, using the X-ray structural data along the magnetite-ulvöspinel series, Bosi et al. (2009) calculated a global instability index value (*i.e.*, the degree to which the structure as a whole is strained) of ~0.10 vu for FeTib3. In accordance with the

bond-valence theory, this value shows the occurrence of strained bonds ascribable to steric effects (Brown 2002) in the ulvöspinel structure.

Implications of out-of-center position of Ti in ulvöspinel

Bond-valence theory, X-ray and neutron structure refinements, in combination with the nuclear density maps, converge to a unified picture: in ulvöspinel, there exists most likely an out-of-center position of Ti at the *M* site, and such a displacement should be shorter than 0.15 Å. This is also supported by the finding of Kunz and Brown (1995): Ti^{4+} is "*found with a bimodal distribution, some structures having no distortion and others having distortion corresponding to an out-of-center shift of about 0.15 Å*".

Under compressional regimes (we consider low-*T* as a compressional regime at a first approximation), we would not expect an exacerbation of this displacement for $^{T}(Fe^{2+})^{M}(Fe^{2+}Ti^{4+})O_4$. According to Yamanaka et al. (2009), the cubic-to-tetragonal phase transition is driven by a Jahn-Teller distortion of the $^{T}Fe^{2+}$ at low-*T* and high-*P*. However, their structural data of high-*P* polymorphs show that the tetrahedron is affected by only a small angular distortion: O-T-O angles vary between 108.3-110.0° (Yamanaka et al. 2009). By contrast, the octahedral distortion is much more pronounced in terms of both bond angles and bond lengths: at 9.8 GPa the difference between the shortest and the longest *M*-O bond distances, $\Delta(M\text{-O})_{max}$, is 0.020 Å, at 10.6 GPa it increased to 0.026 Å, and at 11.4 GPa to 0.030 Å. A similar behavior is observed for the tetragonal polymorph at low-*T*, though with a different magnitude (Yamanaka et al. 2009): at $T<160$ K O-*T*-O angles vary between 109.1-109.7, whereas the distorted octahedron show $\Delta(M\text{-O})_{max}$ of about 0.001 Å at 123 K and 0.004 Å at 103 K.

On the basis of findings of present study, we surmise that, along with the $^{T}Fe^{2+}$ Jahn-Teller distortion recalled by Yamanaka et al. (2009), other factors (*e.g.*, 1st-order Jahn-Teller effect) could drive a polyhedral distortion which dominates the 2nd-order Jahn-Teller behavior in the Ti-occupied *M* site, so driving the high-*P* and low-*T* structural evolution of this mineral.

Acknowledgements

The authors thank the Institut Laue-Langevin (Grenoble, France) for the allocation of neutron beam time. GDG acknowledges the financial support of the Italian Ministry of Education (MIUR) – PRIN 2011, ref. 2010EARRRZ. Financial support from the project PRIN 2010-11 ‘‘GEO-TECH’’, Università Sapienza 2012 “Studio cristallochimico di spinelli appartenenti alle serie $(Mg,Fe)_2TiO_4$, $(Mg,Cu)Al_2O$ e $(Mg,Fe)(Al,Cr)_2O_4$…”, and the Swedish Research Council through the ESF-program EuroMinScl are gratefully acknowledged. S. Mills, K. Lilova and the Technical Editor are thanked for the revision of the manuscript.

References

Akimoto, S. (1954) Thermomagnetic study of ferromagnetic minerals contained in igneous rocks. Journal of Geomagnetism and Geoelectricity, 6, 1–14.

Barth, T. F. W. and Posnjak, E. (1932) Spinel structures: with and without variate atom equipoints. Zeitschrift für Kristallographie, 482, 325-341.

Bosi, F., Hålenius, U., and Skogby, H. (2008) Stoichiometry of synthetic ulvöspinel single crystals. American Mineralogist, 93, 1312–1316.

Bosi, F., Hålenius, U., and Skogby, H. (2009) Crystal chemistry of the magnetite-ulvöspinel series. American Mineralogist, 94, 181–189.

Brown, I.D. (2002) The Chemical Bond in Inorganic Chemistry: the Bond Valence Model, 288 p. International Union of Crystallography Monographs on Crystallography No. 12, Oxford University Press, New York.

Brown I.D. (2009) Recent developments in the methods and applications of the bond valence model. Chemical Reviews, 109, 6858–6919.

Brown, I.D. and Altermatt, D. (1985) Bond-valence parameters obtained from a systematic analysis of the Inorganic Crystal Structure Database. Acta Crystallographica, B41, 244–247.

Campbell, J.W. (1995) LAUEGEN, an X-windows-based program for the processing of Laue diffraction data. Journal of Applied Crystallography, 28, 228-236.

Campbell, J.W., Hao, Q., Harding, M.M., Nguti, N.D., and Wilkinson, C. (1998) LAUEGEN version 6.0 and INTLDM. Journal of Applied Crystallography, 31, 496-502.

Chevallier, R., Bolfa, J., and Mathieu, S. (1955) Titanomagnetites et ilmenites ferromagnétiques. (I) Etude optique, radiocristallographique, chimique. Bulletin de la Societé Francaise de Mineralogie et de Cristallographie, 78, 307–346.

Fujino, K. (1974) Cation distribution and local variation of site symmetry in solid solution series, Fe_3O_4-Fe_2TiO_4. Mineralogical Journal, 7, 472–488.

Farrugia, L.J. (1999) WinGX suite for small-molecule single-crystal crystallography. Journal of Applied Crystallography, 32, 837-838.

Gatta, G.D., Kantor, I., Boffa Ballaran, T., Dubrovinsky, L., and McCammon, C. (2007) Effect of non-hydrostatic conditions on the elastic behaviour of magnetite: an *in situ* single-crystal X-ray diffraction study. Physics and Chemistry of Minerals, 34, 627–635.

Kyono, A., Ahart, M., Yamanaka, T., Gramsch, S., Mao, H.K., and Hemley, R.J. (2011) High-pressure Raman spectroscopic studies of ulvöspinel Fe_2TiO_4. American Mineralogist, 96, 1193–1198.

Kunz, M. and Brown, I.D. (1995) Out-of-center distortions around octahedrally coordinated d^0 transition metals. Journal of Solid State Chemistry, 115, 395-406.

Larson, A.C. (1967) Inclusion of secondary extinction in least-squares calculations. Acta Crystallographica, 23, 664 – 665.

Lenaz, D. and Princivalle, F. (2011) First occurrence of titanomagnetites from the websterite dykes within Balmuccia peridotite (Ivrea-Verbano zone): crystal chemistry and structural refinement. Periodico di Mineralogia, 80, 19–26.

McIntyre, G.J., Lemée-Cailleau, M.-H., and Wilkinson, C. (2006) High-speed neutron Laue diffraction comes of age. Physica B, 385-386, 1055-1058.

Néel, L. (1955) Some theoretical aspects of rock magnetism. Advances in Physics, 4, 191–243.

Millard, R.L., Peterson, R.C., and Hunter, B.K. (1995) Study of the cubic to tetragonal transition in Mg_2TiO_4 and Zn_2TiO_4 spinels by ^{17}O MAS NMR and Rietveld refinement of X-ray diffraction data. American Mineralogist, 80, 885–896.

O'Reilly, W. and Banerjee, S.K. (1965) Cation distribution in titanomagnetites $(1–x)Fe_3O_4$ - xFe_2TiO_4. Physics Letters, 17, 237–238.

Piltz, R.O. (2011) Accurate data analysis for the Koala and VIVALDI neutron Laue diffractometers. Abstracts of the XXII IUCr Congress, Madrid (Spain) 22-30 August 2011. Acta Crystallographica, A67, C155.

Sears, V.F. (1986) Neutron Scattering Lengths and Cross-Sections. In K. Sköld and D.L. Price, Eds., Neutron Scattering, Methods of Experimental Physics, Vol. 23A, 521-550. Academic Press, New York.

Sedler, I.K., Feenstra A., and Peters, T. (1994) An X-ray powder diffraction study of synthetic $(Fe,Mn)_2TiO_4$ spinel. European Journal of Mineralogy, 6, 873–885.

Sheldrick, G.M. (2008) A short history of *SHELX.* Acta Crystallographica, A64, 112-122.

Stout, M.Z. and Bayliss, P. (1980) Crystal structure of two ferrian ulvöspinels from British Columbia. Canadian Mineralogist, 18, 339–341.

Wechsler, B.A., Lindsley, D.H., and Prewitt, C.T. (1984) Crystal structure and cation distribution in titanomagnetites ($Fe_{3-x}Ti_xO4$). American Mineralogist, 69, 754–770.

Wilkinson, C., Khamis, H.W., Stansfield., R.F.D., and McIntyre, G.J. (1988) Integration of single-crystal reflections using area multidetectors. Journal of Applied Crystallography, 21, 471-478.

Yamanaka, T., Mine, T., Asogawa, S., and Nakamoto, Y. (2009) Jahn-Teller transition of Fe_2TiO_4 observed by maximum entropy method at high pressure and low temperature. Physical Review B, 80, 134120.

Yamanaka, T., Kyono, A., Nakamoto, Y., Kharlamova, S., Struzhkin, V.V., and Mao, H-K. (2013) High-pressure phase transitions of $Fe_{3-x}Ti_xO4$ solid solution up to 60 GPa correlated with electronic spin transition. American Mineralogist, 98, 736–744.

Table and Figure captions

Table 1. Details of neutron data collections and refinements of ulvöspinel.

Fig. 1. (F_{obs}-F_{cal})-difference Fourier maps of the nuclear density (fm/Å^3) at z~0.49 phased with the structure model of ulvöspinel (top) *without* the ^{M}Fe and ^{M}Ti sites and (bottom) *with* the ^{M}Fe at (1/2, 1/2, 1/2) and ^{M}Ti at (0.49, 0.49, 0.49) sites. The color scale is different for the two maps.

Fig. 2. Clinographic view of two adjacent FeO_6- and TiO_6-octahedra in the structure of ulvöspinel. For the TiO_6-polyhedron: Ti fixed at (0.49, 0.49, 0.49); the dashed line represents the axis upon which the special position (1/2, 1/2, 1/2) lies. Displacement ellipsoid probability factor: 90%, based on the structure refinement of this study.

Fig. 3. Finite bond network graphs for ulvöspinel $^{T}(Fe^{2+})^{M}(Fe^{2+}Ti^{4+})O_4$: (a) random distribution of the valences 2+ and 4+ over the M sites, yielding a mean valence of 3+; (b) order distribution of 2+ and 4+ at M1 and M2. The numbers are theoretical bond valences predicted using the two network equations (see text; Brown 2002).

Fig. 4. Cluster of octahedra in the spinel structure: (a) cluster formed by short-range arrangement (Fe-Fe-Fe)$^{\Sigma 6+}$-(Ti^{4+})-(Ti-Ti-Ti)$^{\Sigma 12+}$; (b) cluster formed by arrangement (Fe-Fe-Ti)$^{\Sigma 8+}$-(Ti^{4+})-(Fe-Ti-Ti)$^{\Sigma 10+}$. Both cases result in asymmetric charge distributions, so that the cation-cation repulsions do not cancel and the "central" (Ti^{4+}) may be displaced from the center of its octahedron.

Table 1. Details of neutron data collections and refinements of ulvöspinel.

Sample FeTib3	Crystal #1	Crystal #2
Crystal shape	Octahedron	Octahedron
Crystal size (mm^3)	2.8 x 2.1 x 2.0	3.2 x 2.3 x 2.2
Crystal colour	Black	Black
Unit-cell constant (Å)	8.5139(5)	8.5139(5)
Chemical formula (EMPA-WDS)	$Fe^{3+}_{0.40}Fe^{2+}_{1.80}Ti_{0.80}O_4$	$Fe^{3+}_{0.40}Fe^{2+}_{1.80}Ti_{0.80}O_4$
Space Group	$Fd\bar{3}m$	$Fd\bar{3}m$
Z	8	8
T (K)	298	298
Radiation	Polychromatic, neutron	Polychromatic, neutron
Diffractometer	VIVALDI, Laue diffractometer	VIVALDI, Laue diffractometer
$\lambda_{min}/\lambda_{max}$ (Å)	0.78 / 5.2	0.78 / 5.2
d_{min} (Å)	0.48	0.48
	$1 \le h \le 17$	$1 \le h \le 17$
	$0 \le k \le 12$	$0 \le k \le 12$
	$0 \le l \le 11$	$0 \le l \le 11$
No. measured reflections	8338, merged to 212	5550, merged to 210
No. unique reflections	135	134
No. unique refl. with $F_o > 4\sigma(F_o)$	129	129
No. refined parameters	9	9
R_{int}	0.0224	0.0187
R_1 *(F)* with $F_o > 4\sigma(F_o)$	0.0312	0.0324
R_1 *(F)* for all the unique reflections	0.0331	0.0347
wR_2 *(F^2)*	0.0676	0.0553
S	3.980	3.290
Weighting Scheme: *a*, *b*	0.01, 0	0.01, 0
Residuals (fm/Å^3)	+0.50/-0.55	+0.53/-0.57
u	0.25997(5)	0.26006(4)
T-O (Å)	1.9904(7)	1.9917(6)
M-O (Å)	2.047(1)	2.046(1)
U_{11} (O) (Å^2)	0.0149(1)	0.0150(1)
U_{23} (O) (Å^2)	-0.00252(8)	-0.00268(6)
U_{11} (*T*) (Å^2)	0.0112(1)	0.0112(1)
U_{11} (*M*) (Å^2)	0.0082(2)	0.0078(2)
U_{23} (*M*) (Å^2)	-0.0005(1)	-0.0008(1)
^{M}Ti *s.o.f.*	0.865(5)	0.888(4)
Refinement with Ti at 0.49,0.49,0.49		
No. refined parameters	9	
R_1 *(F)* with $F_o > 4\sigma(F_o)$	0.0318	
R_1 *(F)* for all the unique reflections	0.0337	
wR_2 *(F^2)*	0.0686	
S	4.041	
Weighting Scheme: *a*, *b*	0.01, 0	
Residuals (fm/Å^3)	+0.50/-0.54	
u	0.25997(8)	
T-O (Å)	1.990(1)	
M-O (Å)	2.047(1)	
U_{11} (O) (Å^2)	0.0149(2)	
U_{23} (O) (Å^2)	-0.0025(1)	
U_{11} (*T*) (Å^2)	0.0112(2)	
U_{11} (*M*) (Å^2)	0.0103(3)	
U_{23} (*M*) (Å^2)	0.0015(1)	
Ti *s.o.f.*	0.866(8)	
U_{iso} (Ti) (Å^2)	0.0089*	
Ti – O' (Å)	1.9585(7)	
Ti – O'' (Å)	2.1421(8)	
Ti – ^{M}Fe (Å)	0.147	

Note: $R_{int} = \Sigma \mid F_{obs}^2 - F_{obs}^2(\text{mean}) \mid / \Sigma [F_{obs}^2]$; $R_1 = \Sigma||F_{obs}| - |F_{calc}||/\Sigma|F_{obs}|$;
$wR_2 = [\Sigma[w(F^2_{obs} - F^2_{calc})^2]/\Sigma[w(F^2_{obs})^2]]^{0.5}$, $w = 1/[\sigma^2(F_{obs}^2) + (aP)^2 + bP]$, $P = (\text{Max}(F_{obs}^2, 0) + 2F_{calc}^2)/3$;
$S = \{\Sigma[w(F_{obs}^2 - F_{cal}^2)^2]/(n\text{-}p)\}^{1/2}$, n is the number of reflections and p is the total number of parameters refined. Origin fixed at $\bar{3}$m. Unit-cell constants from the X-ray study (see text for details). EMPA-WDS data from Bosi et al. (2009). *Fixed after the first cycles of refinement.

Fig. 1. (F_{obs} – F_{cal})-difference Fourier maps of the nuclear density (fm/Å^3) at z ~0.49 phased with the structure model of ulvöspinel (top) *without* the ^{M}Fe and ^{M}Ti sites and (bottom) *with* the ^{M}Fe at (1/2, 1/2, 1/2) and ^{M}Ti at (0.49, 0.49, 0.49) sites. The color scale is different for the two maps.

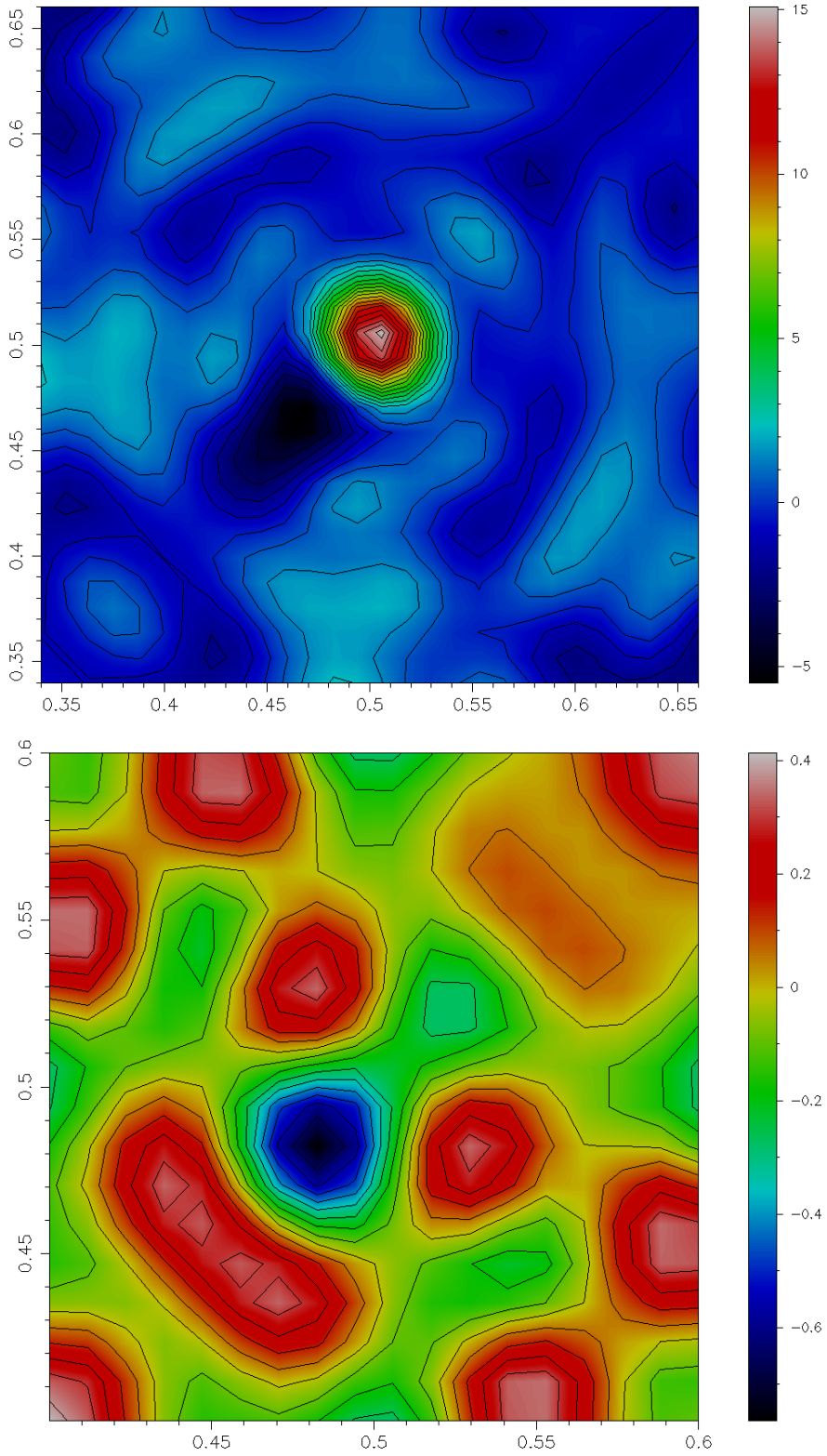

(Fig. 1, B&W)

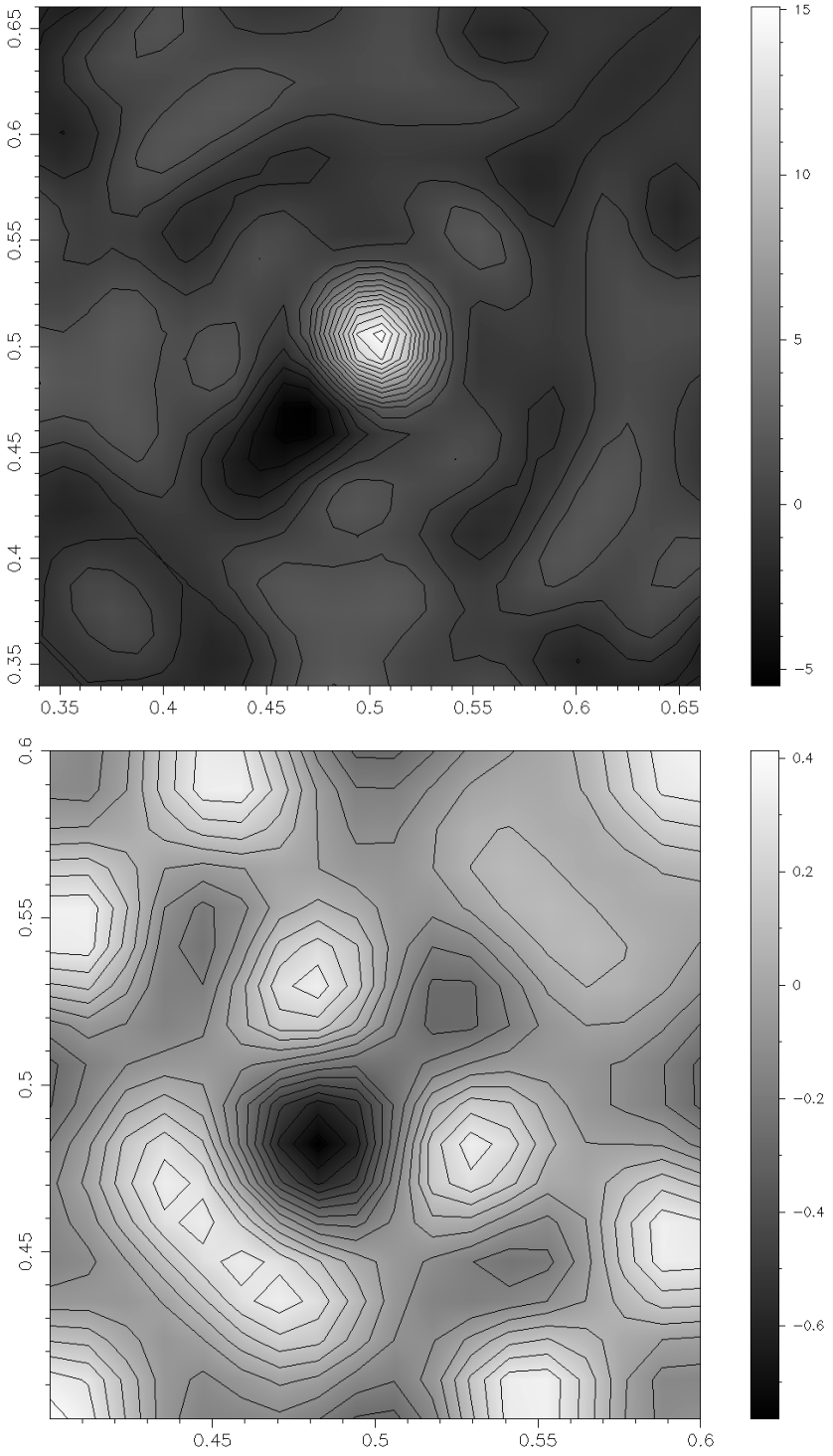

Fig. 2. Clinographic view of two adjacent Fe- and Ti-octahedra in the structure of ulvöspinel. For the Ti-polyhedron: Ti fixed at 0.49, 0.49, 0.49; the dashed line represents the axis upon which the special position 1/2, 1/2, 1/2 lies. Displacement ellipsoid probability factor: 90%, based on the structure refinement of this study.

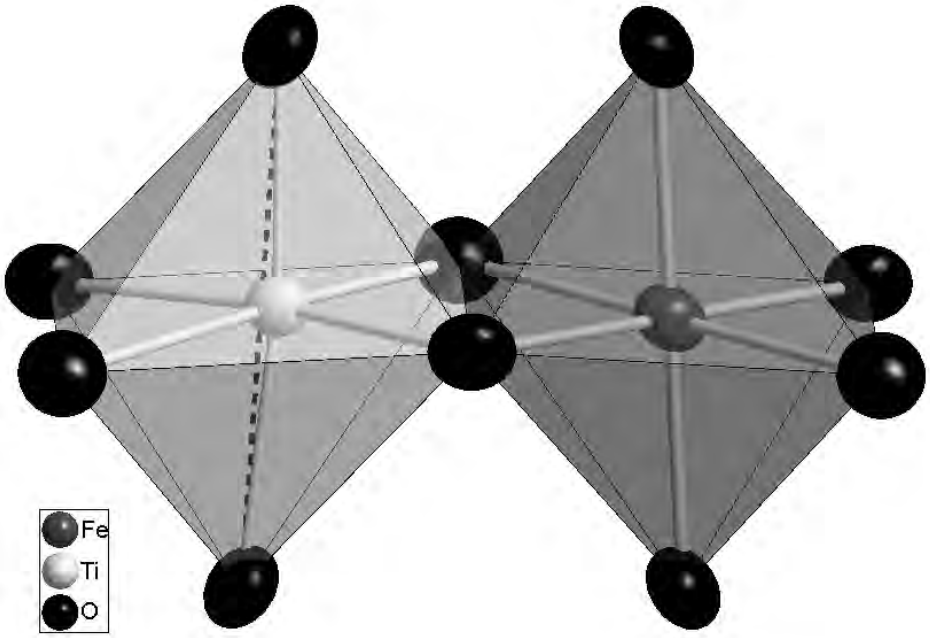

Fig. 3. Finite bond network graphs for ulvöspinel $^{T}(Fe^{2+})^{M}(Fe^{2+}Ti^{4+})O_4$: (a) random distribution of the valences 2+ and 4+ over the *M* sites, yielding a mean valence of 3+; (b) order distribution of 2+ and 4+ at *M*1 and *M*2. The numbers are theoretical bond valences predicted using the two network equations (see text; Brown 2002).

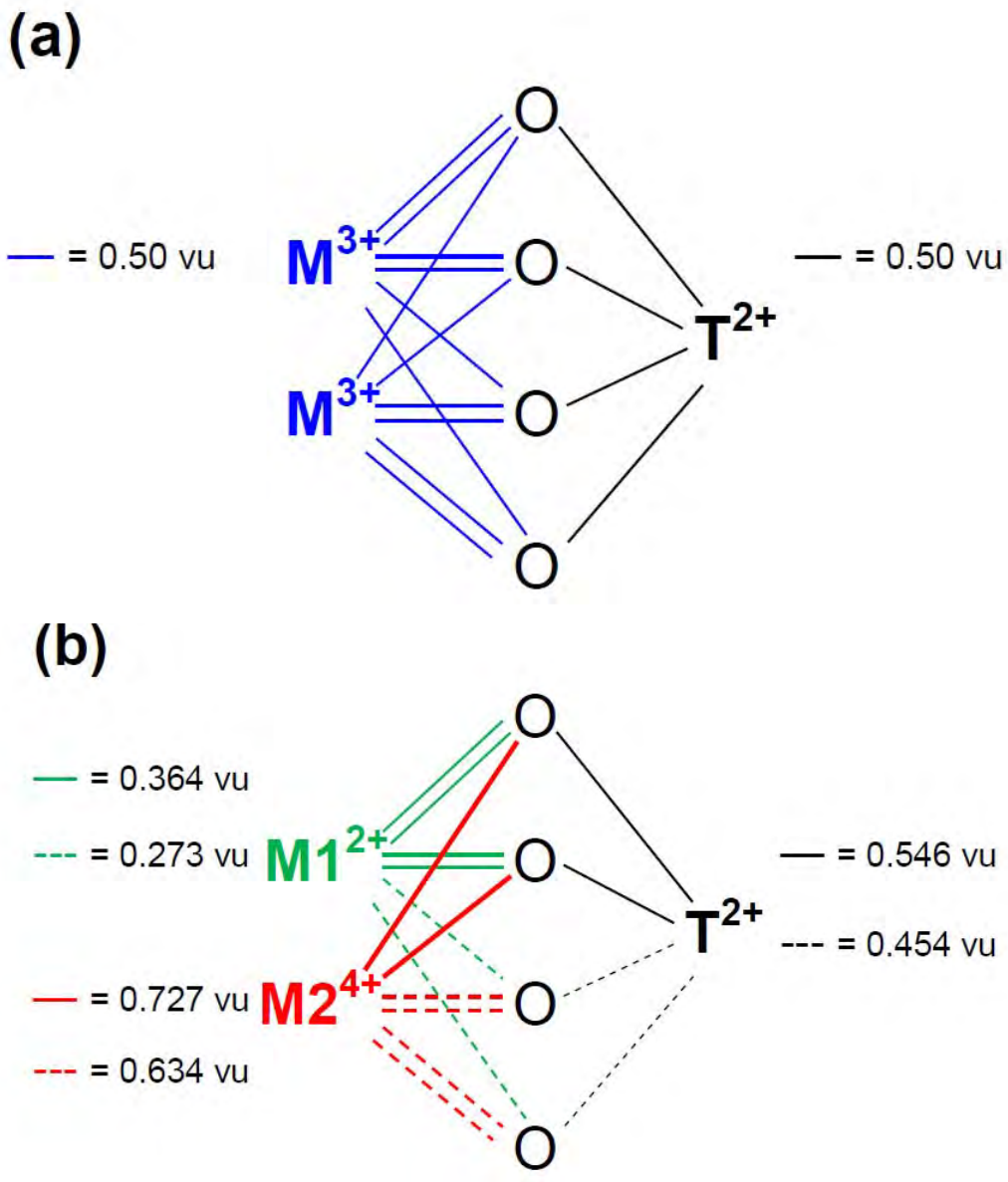

(Fig. 3, B&W)

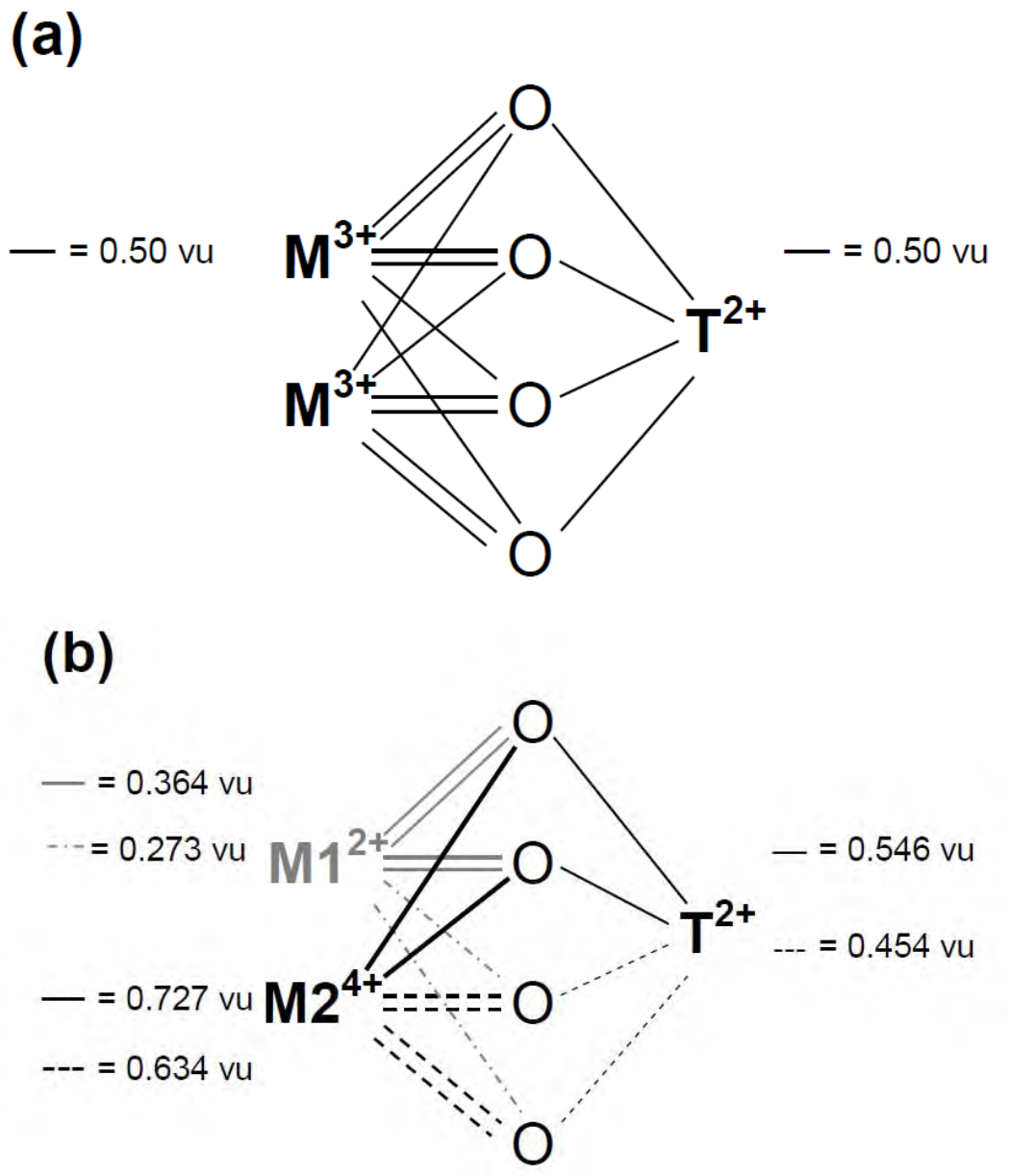

Fig. 4. Cluster of octahedra in the spinel structure: (a) cluster formed by short-range arrangement (Fe-Fe-Fe)$^{\Sigma 6+}$-(Ti^{4+})-(Ti-Ti-Ti)$^{\Sigma 12+}$; (b) cluster formed by arrangement (Fe-Fe-Ti)$^{\Sigma 8+}$-(Ti^{4+})-(Fe-Ti-Ti)$^{\Sigma 10+}$. Both cases result in asymmetric charge distributions, so that the cation-cation repulsions do not cancel and the "central" (Ti^{4+}) may be displaced from the center of its octahedron.

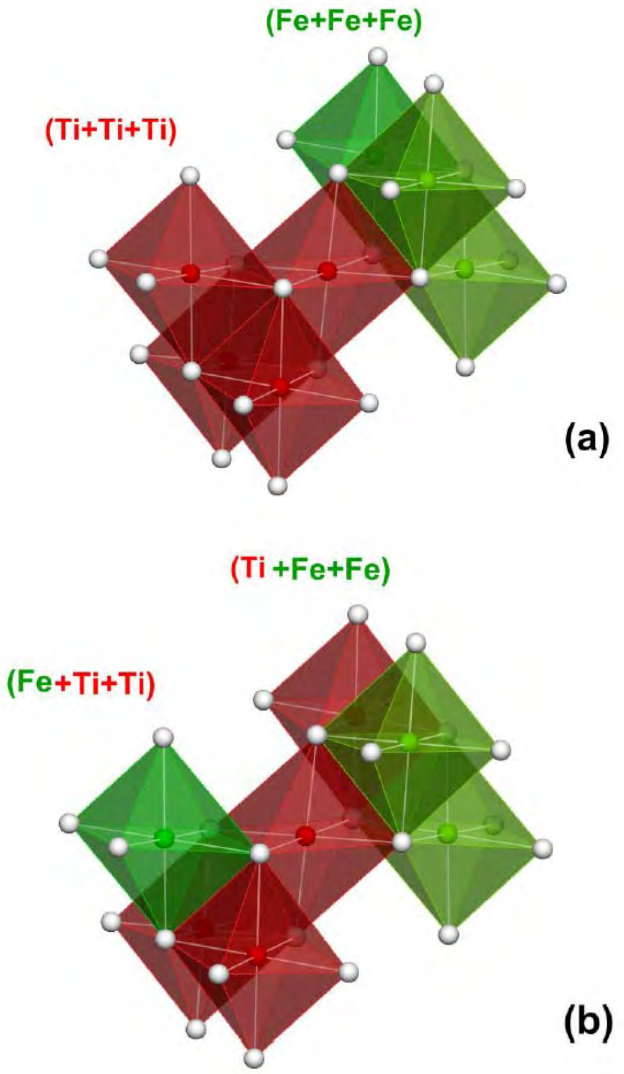

(Fig. 4, B&W)

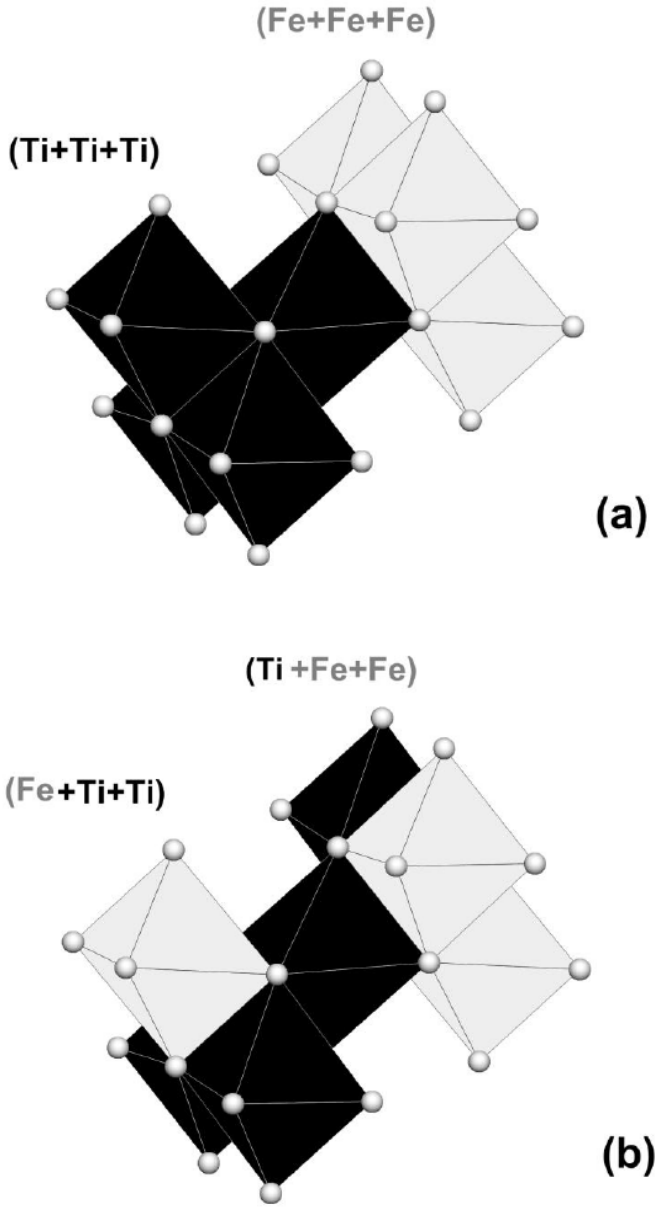

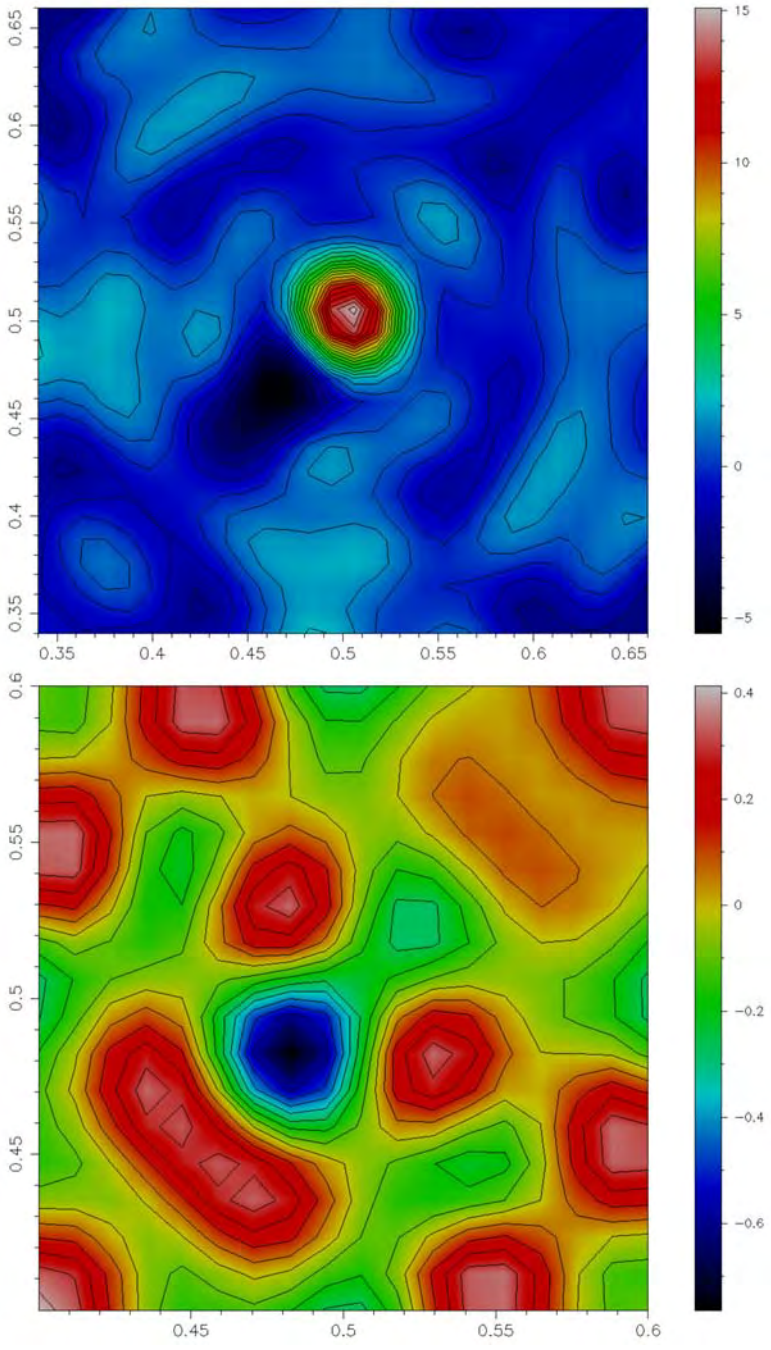
0.65
0.6
0.55
0.5
0.45
0.4
0.35
0.35
0.4
0.45
0.5
0.55
0.6
0.65
15
10
5
0
−5
0.6
0.55
0.5
0.45
0.45
0.5
0.55
0.6
0.4
0.2
0
−0.2
−0.4
−0.6

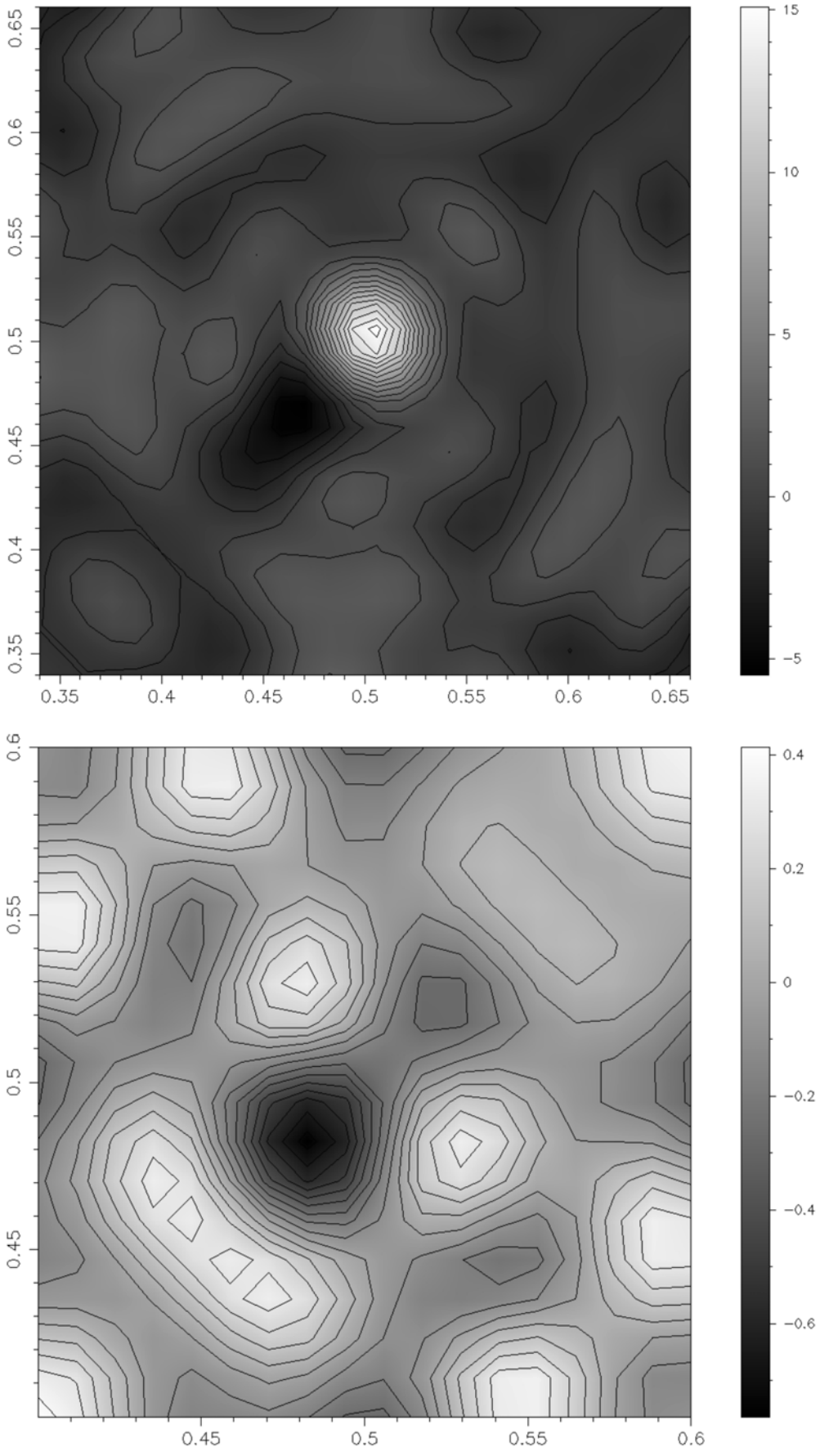
0.65
0.6
0.55
0.5
0.45
0.4
0.35
0.35
0.4
0.45
0.5
0.55
0.6
0.65
15
10
5
0
−5
0.6
0.55
0.5
0.45
0.45
0.5
0.55
0.6
0.4
0.2
0
−0.2
−0.4
−0.6

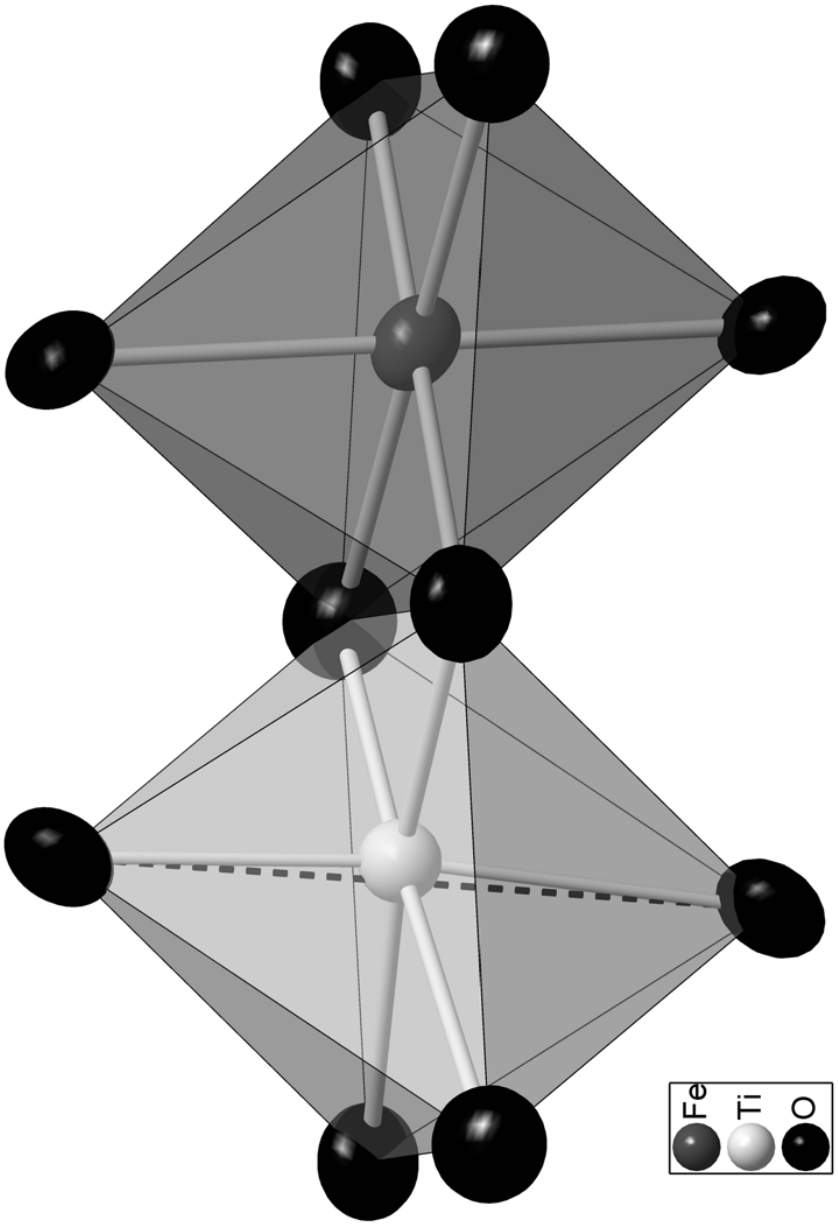
Fe
Ti
O

Figure 3

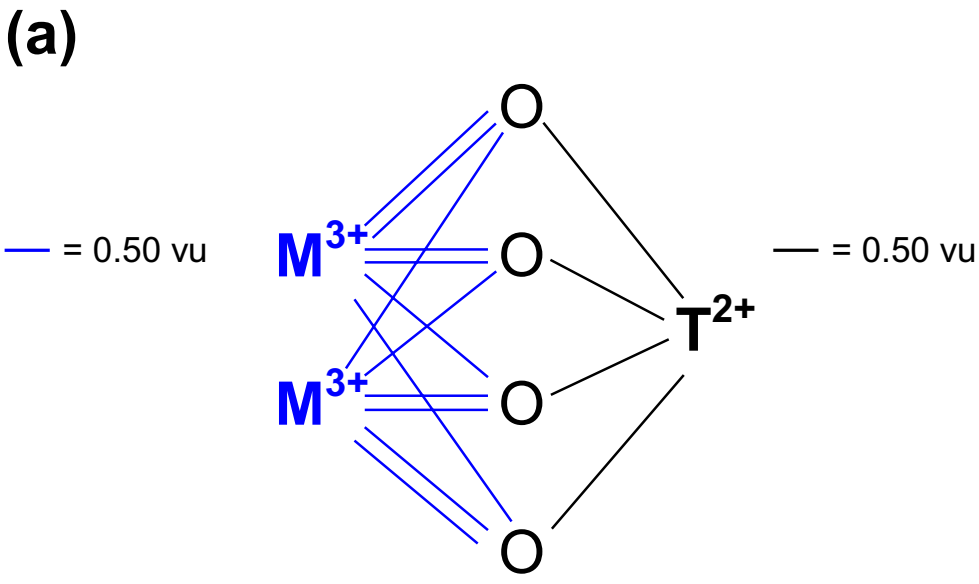

Figure 3

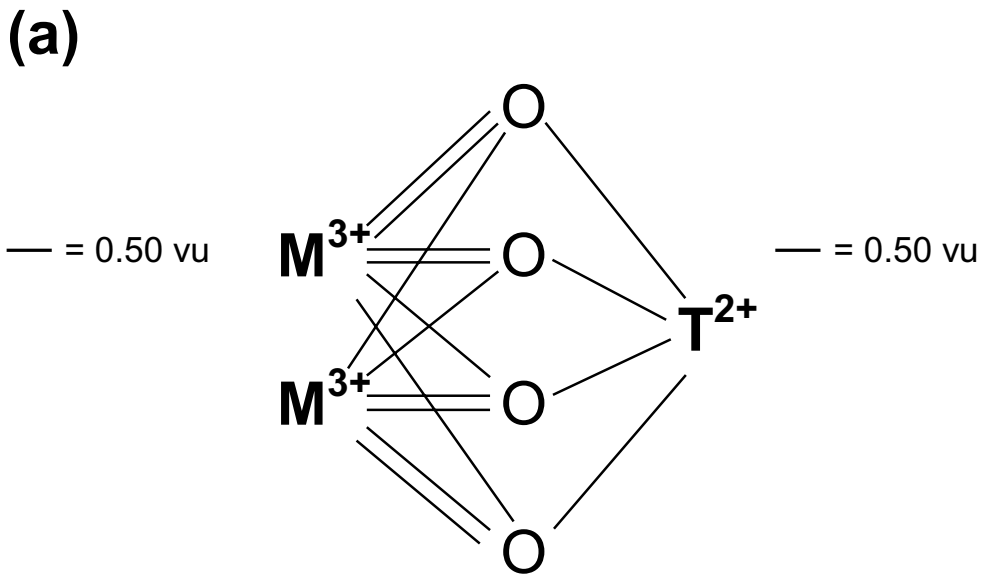

Figure 3

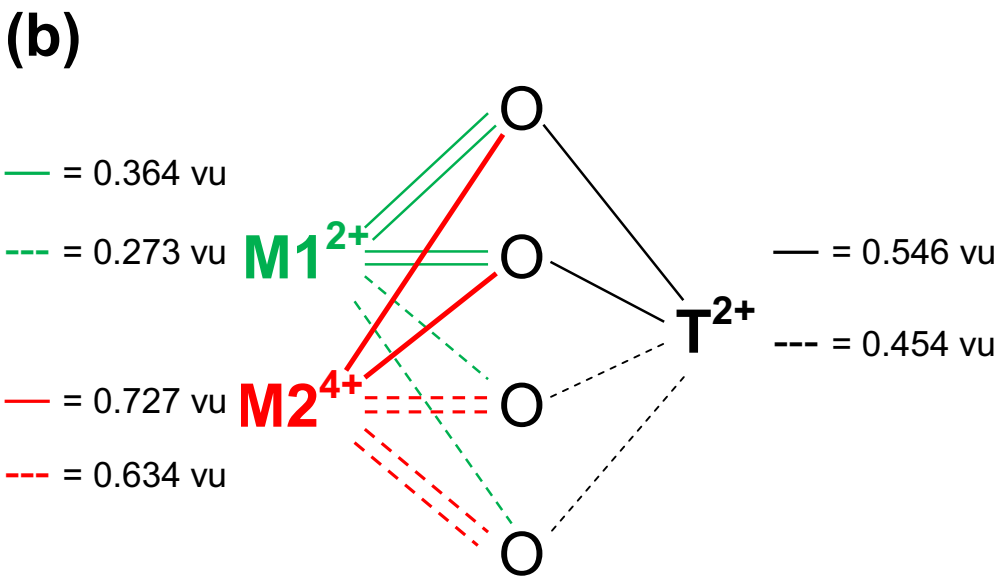

Figure 3

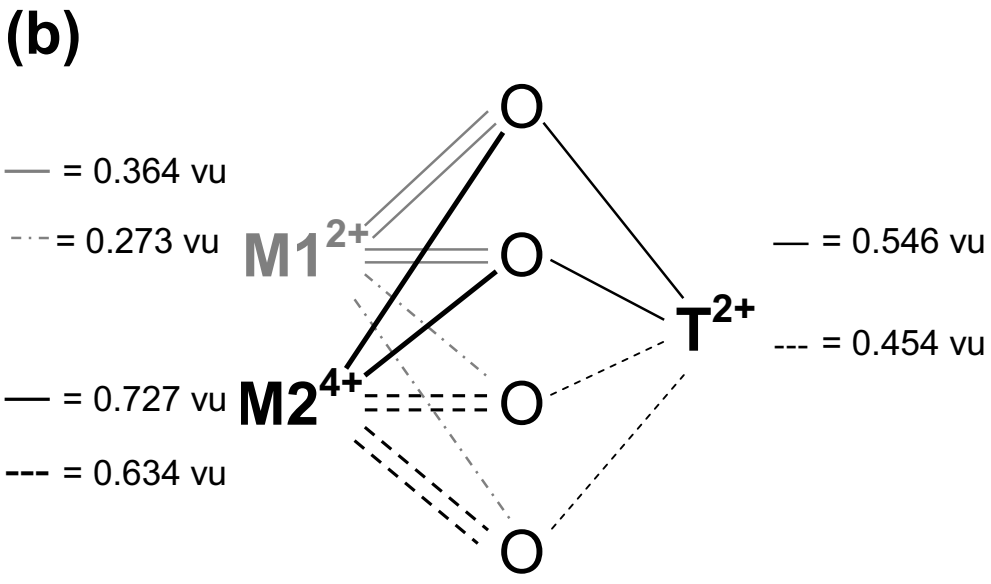

Figure 4

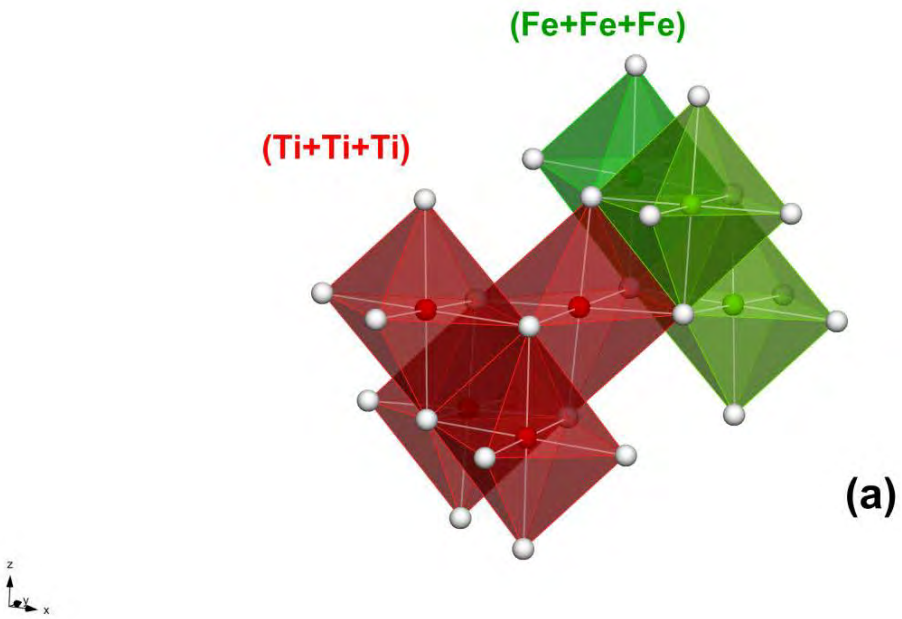

Figure 4

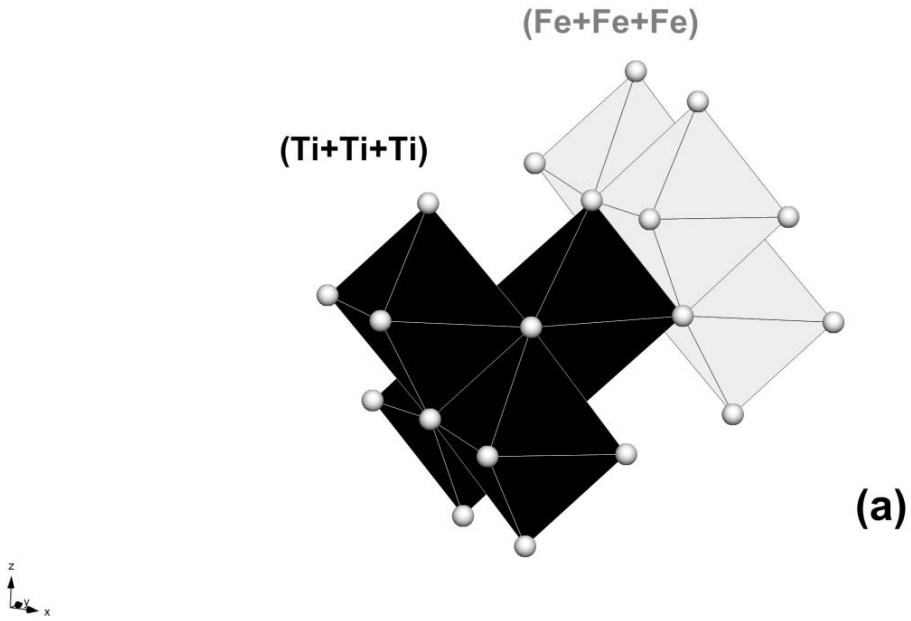

Figure 4

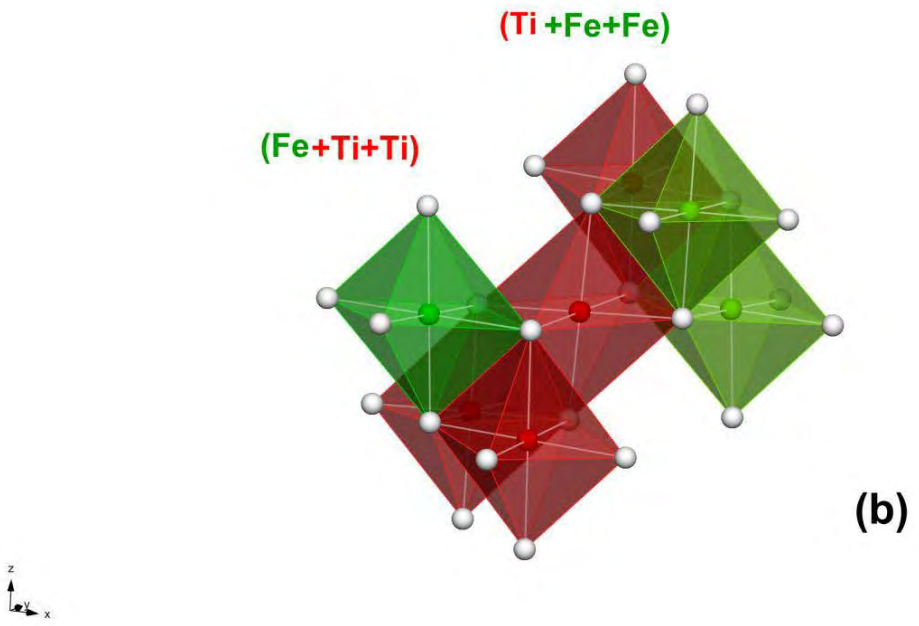

Figure 4